Materials Transactions, Vol. 58, No. 5 (2017) pp. 817 to 824

Morphology Evolution of γ' Precipitates during Isothermal Exposure in Wrought Ni-Based Superalloy Inconel X-750

Hiromu Hisazawa[1,*], Yoshihiro Terada[2] and Masao Takeyama[3]

[1]*Department of Materials Science and Engineering, Interdisciplinary Graduate School of Science and Engineering, Tokyo Institute of Technology, Yokohama 226–8502, Japan*
[2]*Department of Materials Science and Engineering, School of Materials and Chemical Technology, Tokyo Institute of Technology, Yokohama 226–8502, Japan*
[3]*Department of Materials Science and Engineering, School of Materials and Chemical Technology, Tokyo Institute of Technology, Tokyo 152–8552, Japan*

The morphological evolution of γ' precipitates and lattice misfit with isothermal aging were closely investigated in wrought Ni-based superalloy Inconel X-750. The γ' morphology dramatically changes in terms of shape, distribution, coalescence and coherency at the γ/γ' interface. These processes and their dependence on temperature are summarized as a γ' morphology map together with a time–temperature–precipitation (TTP) diagram through quantifying relevant morphological parameters. The lattice misfit was measured by X-ray diffraction and is positive; it decreases from 0.6% at room temperature to 0.1% at the aging temperature. These results suggest that the morphological changes of the γ' precipitates are attributable to very low lattice misfit, the interaction of the elastic field, the volume fraction of the precipitates and incoherence in γ/γ' interface. [doi:10.2320/matertrans.M2016376]

(Received October 25, 2016; Accepted January 19, 2017; Published April 7, 2017)

Keywords: *nickel-based alloy, gamma prime, morphology, lattice misfit*

1. Introduction

Compared to other classes of high-temperature materials, Ni-based superalloys exhibit excellent high-temperature strength retained at high fractions of their melting temperature. This is a great advantage for power engineering applications such as gas turbine[1)] and advanced ultra-super-critical (A-USC) power plant to improve fuel efficiency for sustainable development.

This high-temperature performance is due to the presence of $L1_2$ ordered γ' precipitates from face-centered cubic (fcc) γ matrix with certain constrained lattice misfit. Ni-based superalloys are considered promising materials for increase in operating temperature and/or time in A-USC applications, many of these materials have recently been screened using long-term creep tests[2,3)]. However, this screening has revealed that not all alloys have sufficient long- and short-term strength. The equipment in an A-USC plant, e.g., main steam tubes, are exposed to high temperature conditions for a long time more than 30 years, and clarifying the long-term creep strength of the materials used in such components is important.

We believe that the most alloys have lower long-term strength because of microstructural instability of γ' precipitates in their γ matrix[4,5)]. Cast Ni-based superalloys, which have been used in environments with extremely high temperatures, exhibits good microstructural stability despite their high volume fraction of γ' precipitates. The morphology of the γ' precipitates is cuboidal, and each particle is orderly aligned. Here we speculate that the morphology of γ' particles strongly depends on the lattice misfit between the γ matrix and the γ' precipitates in the Ni-based superalloy at high temperatures. Lattice misfit δ is derived by the following equation representing the difference ratio of the lattice parameters of the γ and γ' phases:

$$\delta = \frac{a_{\gamma'} - a_{\gamma}}{a_{\gamma}} \tag{1}$$

where $a_{\gamma'}$ and a_{γ} are the lattice parameters of the γ and γ' phases, respectively. Lattice misfit δ usually represents the degree of constraint elastic strain between coherent γ and γ' phases. The authors of numerous studies have reported that the elastic strain due to lattice misfit has strongly affects the kinetics of microstructure degradation and γ' morphology[6–10)]. For instance, the shape of the γ' particles changes from spherical to a cuboidal and a flat and narrow channel between γ and γ' phases is stabilized. The γ' particles coarsen faster in alloys with the high lattice misfit than in ones with the low lattice misfit. This dependency suggests the possibility of developing a novel concept that wrought Ni-based superalloy with a low volume fraction of γ' precipitates by controlling lattice misfit at temperatures near the service temperature.

The term "γ' morphology" generically refers to numerous properties of γ' precipitates. In particular, the γ' shape attracts extensive interest and has been widely studied for optimization of the mechanical properties of alloys. The γ' precipitates often evolve from an initial spherical shape to a cuboidal one, consistent with theoretical approaches indicating that precipitation shape strongly depends on particle size[11–15)]. Many alloys with fcc crystal structure have an elastically soft <100> direction and a hard <111> direction. The γ/γ' interface tends to form parallel to the {100} plane to retain elastic strain energy, resulting in a cuboidal γ' particle shape when its size becomes sufficiently large. Some particles form a rod- or plate-like shape under the influence of high levels of misfit and external stresses as so called rafting. The various shape parameters have also been used to quantify of the γ' morphology with reasonable objectivity. Fährmann *et al.*[9)] derived the aspect ratio A and a stereological parameter, S_{ster}, to quantify

*Corresponding author, E-mail: hisazawa.h.aa@m.titech.ac.jp

the morphological evolution of γ' shapes from spherical to cuboidal:

$$S_{\text{ster}} = \frac{P_{\text{i}} - P_{\text{s}}}{P_{\text{c}} - P_{\text{s}}} \tag{2}$$

where P_{i} is the measured perimeter of the particle, and P_{c} and P_{s} are measured perimeters of an area-equivalent circle and square, respectively. Stereological parameter S_{ster} can be used only when we assume particle γ' particle shapes are equiaxed because of its dependency on aspect ratio A.

Prikhodko *et al.*[16] derived a shape parameter, termed Σ, for measuring the shape of γ' particles in as-aged Ni-based alloys:

$$\Sigma = \frac{A_{\text{p}} - A_4}{0.5708 A_4} \tag{3}$$

where A_{p} and A_4 are the measured particle area and area of the largest four-sided polygon inscribed within the particle, respectively. The empirical constant 0.5708 was used to normalize measured values between 0 and 1. The magnitude of Σ, unlike that of S_{ster}, is independent of the particle aspect ratio; however γ' particles shapes other than the vertices of the four-sided polygon are not reflected. Thus, a need exists for the developing of new parameters expressing the shape of γ' particles.

However, Maheshwari *et al.*[17] and Lund *et al.*[18] qualitatively reported that γ' particles interact among themselves, resulting in a heterogeneous dispersion and abnormal coarsening of γ' particles. This tendency is supported by Zhao *et al.*[19] and Su *et al.*[20], who performed calculations concerning the elastic strain field around γ' particles. Small γ' volume fractions are preferred for observing evidence of interactions among γ' particles. Moreover, some alloys have irregularly shaped γ' particles or ones with a broad size distribution because of coalescence of γ' particles after long-term aging[21]. These results strongly suggest that not only the shape, but also the dispersion and coalescence should be considered simultaneously when evaluating the γ' morphology. A quantitative evaluation, such as the determination of the shape parameter is also required.

The aim of the present study is to demonstrate the simultaneous quantification of the change in the morphology of γ' precipitates upon isothermal aging in terms of the shape, dispersion and coalescences. The shape parameter is newly applied to a wrought Ni-based superalloy. Two parameters were also developed to evaluate dispersion and coalescence. The change in lattice misfit with aging is also measured to clarify their relationship in a simple wrought Ni-based superalloy.

2. Experimental Procedure

2.1 Materials

Wrought Ni-based superalloy Inconel X-750 was used in this study. Table 1 shows the chemical composition of the alloy. This alloy has a relatively simple composition and consists predominantly of γ and γ' phases within grains and a relevant volume fraction of γ' phase particles (5–20 vol%) in the γ matrix[22–26]. We can easily ignore the small amount of blocky carbide or plate-shaped eta intermetallic phase at the grain boundary, which weakly affects the γ' phase within grains[27]. The alloy was cut from a 250-mm-diameter forged bar into $10 \times 10 \times 10$ mm^3 cubes. They were solution treated at 1423 K for 4 h and then water-quenched to obtain a complete γ single phase microstructure. The grain size was approximately 170 μm after solution treatment and unchanged during subsequent heat treatments. Aging was carried out isothermally at 973–1173 K for up to 4000 h in air. Samples were also cut into $1 \times 10 \times 10$ mm^3 plates for use in various experiments.

2.2 Microstructure observation

Microstructure observation was conducted by using field-emission scanning electron microscopy (FE-SEM) and transmission electron microscopy (TEM). As solution treated and aged specimens for FE-SEM were prepared by the conventional metallographic technique and by slight electronic etching with phosphoric acid saturated with chromium(VI) oxide. The volume fraction of the γ' phase was also measured by SEM secondary electron image (SEM-SEI) and image processing. Notably, electric etching dissolves the γ matrix leaving γ' precipitates, resulting in an over-estimation of the γ' volume fraction; however, enable us to evaluate the shape of γ' particles stereologically. The γ' particle size (d) was also measured via SEM-SEI as the average length of the major and minor axes. Aged specimens for TEM were prepared from discs by the twin-jet polishing technique and a 10% perchloric acid ethanol solution.

2.3 Quantification of γ' morphology

2.3.1 Shapes

γ' particle shape was assumed to be intermediate between spheres and cubes or irregular shapes. Their shape was evaluated by the fastest and objective technique: the moment invariant method developed by MacSleyne *et al.*[28] Absolute moment invariant ω_2 was selected to evaluate the cuboidal magnitude according to the precedent for commercial alloys with a large volume fraction[29,30]. The ω_2 was converted into simple shape parameter η because the shape corresponding to ω_2 is difficult to understand. Figure 1 shows a schematic of the assumed γ' particle shape used to define the shape param-

Table 1 Chemical composition of Inconel X-750.

Inconel X-750	Ni	Cr	Fe	Ti	Al	Nb	C
mass%	Bal.	14.9	6.58	2.49	0.79	1.00	0.04
at%	Bal.	16.2	6.96	2.95	1.66	0.61	0.19

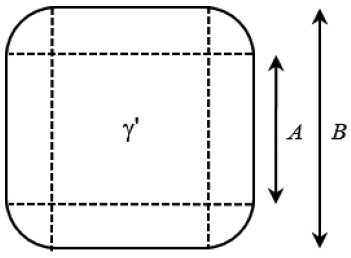

Fig. 1 Schematic of the γ' particles observed in Ni-based superalloys. Note that shape parameter $\eta = A/B$ becomes zero when the γ' particle is spherical in shape, whereas a perfect cuboidal particle results in $\eta = 1$.

eter given by eq. (4):

$$\eta = \frac{A}{B}. \tag{4}$$

Shape parameter η is the ratio of length A and distance B of a flat interface; ω_2 is derived as eq. (5):

$$\omega_2 = \frac{144\left(\pi(\eta-1)^2 - 4\eta(\eta-2)\right)^4}{\left(3\pi(\eta-1)^2(1-2\eta+5\eta^2) - 16\eta(3\eta^3-7\eta^2+6\eta-3)\right)^2} \tag{5}$$

The range of ω_2 is 144 to $16\pi^2$ when the shape described in Fig. 1 is assumed, and gives a shape parameter η value between 0 and 1. For instance, $\eta = 0$ indicates a complete sphere or ellipsoid and $\eta = 1$ ideally means complete polyhedron including cuboid.

In this study, an irregular shape is defined as "cave" shape such as fan-like or flower-like particles as shown in Fig. 3(d). Irregular shape particles were formed as a result of coalescence and they were detected by jumping the ω_2 from a value between 144 and $16\pi^2$ to values between 0 and 144[28]. The value of η was set to zero when the ω_2 was less than 144. Carbide and eta intermetallic phases were rarely observed and were excluded manually because they are detected at high η through moment invariant technique corresponding to more cuboidal one.

2.3.2 Dispersion

Some of the γ' particles interact and undergo a change in morphology. Here, we use the term "group" to refer to a group of particles whose shape appears to be a result of particle interaction, such as, particle that we refer to as, being aligned or arrayed. The fraction of interacting particles is quantified as:

$$\nu = \frac{N^*}{N} \tag{6}$$

where N and N^* are the normal and group particle density and ν is the dispersion parameter, respectively. The group of interacting particles is defined as those satisfying three conditions: 1) They have flat and facing γ/γ' interfaces; 2) they do not appear to be overlapped along to the observed direction; 3) their channel is sufficient narrow. The condition "sufficient narrow" is defined as follows: For two neighboring particles, we draw area-equivalent circles with the same center positions as the particles; when the two circles touch each other, condition 3 is satisfied. This condition is calculated using eq. (7).

$$l_{ij} \le \frac{d_i + d_j}{2} = \sqrt{\frac{A_i}{\pi}} + \sqrt{\frac{A_j}{\pi}} \tag{7}$$

where l_{ij} is the distance between centers of the γ' particles, d_i and d_j are the equivalent circle diameters and A_i and A_j are the areas of the particles respectively. The positions of the centers and areas of the particles were experimentally obtained to determine whether they satisfy condition 3. $\nu = 0$ indicate all of particles form a group as a result of the interaction and $\nu = 1$ indicates all particles are isolated.

2.3.3 Coalescence

Here, we define coalescence as the merging of particles and the formation of a new large particle. In terms of kinetics, this process represents alternative coarsening mode; thus, we can detect it as a statistical size distribution parameter. To examine the effect of coalescence of the precipitates on the particle size distribution, the normalized standard deviation was used as the representative coalescence parameter σ^* in this study:

$$\sigma^* = \frac{1}{\bar{d}}\sqrt{\sum_i \frac{\left(d_i - \bar{d}\right)^2}{n-1}} \tag{8}$$

where d_i and $\bar{d}$ are individual and average particle sizes, respectively, and n is the number of measured particles. This parameter σ^* becomes constant at 0.219 with isothermal aging when we assume pure Ostwald ripening, whose driving force is only reduction of interfacial energy. Parameter σ^* can be reasonably used to detect different coarsening modes, such as coalescence, as an increase of σ^*.

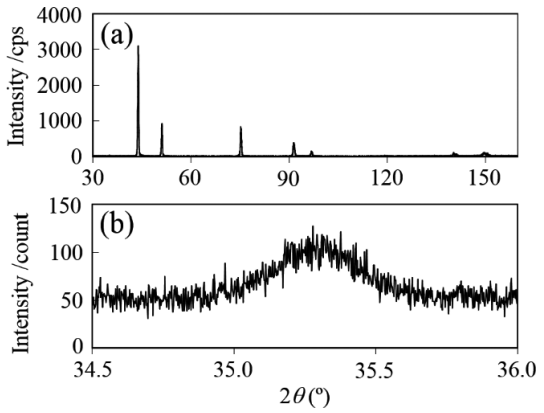

Fig. 2 XRD profile of Inconel X-750 aged at 1173 K/1000 h (a). The region around 35° of (a) is magnified in (b), which indicates the 110 superlattice peak of the γ' precipitates.

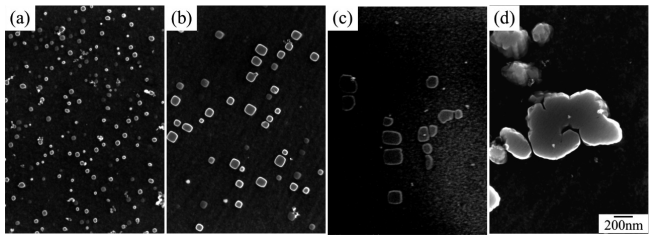

Fig. 3 FE-SEM micrographs of Inconel X-750 aged at 1173 K for 1 h (a), 10 h (b), 96 h (c) and 1000 h (d).

2.4 X-ray diffraction

Lattice parameters of γ and γ' phases were measured by the laboratory-scale X-ray diffraction (XRD) technique. Generally, measuring lattice misfit of wrought Ni-based superalloy with low lattice misfit and a small volume fraction of precipitate is difficult because of very weak superlattice intensity[31]. Fundamental peaks of the matrix and precipitates are also completely overlapped. Extremely bright synchrotron X-rays or numerical peak deconvolution methods have been used to measure lattice misfit[32]. We succeeded to detect 110 superlattice peak at approximately 35° 2θ using a very long exposure time. The accurate geometry is described as follows. An example of a whole XRD profile (Fig. 2(a)) and a magnified view of the 110 peak (Fig. 2(b)) are shown. The lattice pa-

rameter of the γ matrix was determined from the fundamental peak position and the intercept with Nelson–Riley function, whereas that of the γ' precipitate was obtained from the 110 peak. Bulk specimens for XRD were prepared to avoid lattice strain induced by grinding or microstructural changes induced by annealing. The specimens were finally deep electrically polished to relieve the chemical changes and dislocation induced during mechanical polishing. The X-ray diffractometer was configured with parallel beam geometry, which enables measurement of peak positions with very small error. High-temperature XRD was also conducted at temperatures up to 1173 K under flowing helium gas. The specimen was heated from lower to higher temperature in steps of 100 K. High-temperature XRD measurements conducted 15 min after the samples reached the set temperature. The measurement at each step required approximately 8 h.

3. Results

3.1 Microstructure

Figure 3 shows the SEIs of the alloy aged at 1173 K from 1 to 1000 h. Coarsening of the γ' particles began at 1173 K/1 h. The particle size increased and particle number density decreases with aging. The shape of γ' particles in the specimen aged for 1 h is spherical. The shape becomes cuboidal for the 10 h aged specimen and becomes spherical again after 96 h of aging. In the case of aging times longer than 1000 h, the shape of γ' particles changes to irregular. The γ' particles are incoherence and have coalesce in the 1000 h aged specimen. In terms of the dispersion, the γ' particles for the specimens aged for 1–10 h are almost homogeneously dispersed; however, for the 96 h aged specimen the distribution of γ' particles are heterogeneous; some particles are neighboring each other. The γ' particles for the 1000 h aged specimen are homogeneously dispersed again as the result of coalescence of neighboring particles.

Figure 4 shows SEIs of the alloy aged at 1073 K. They show a similar tendency except for larger volume fractions of precipitates. The 1 h aged specimen shows a spherical shape and a homogeneous dispersion, the 24 h aged samples shows a relatively cuboidal shape and the 750 h aged samples shows aligned particles. The order of change in γ' morphology is almost the same as that observed in the samples aged at 1173 K, although its kinetics is much slower. This result is consistent with the temperature dependence of the diffusion rate. A larger volume fraction of γ' phase is achieved at lower aging temperatures.

Figure 5 shows the change in the particle size and in the area fraction of the γ' precipitate obtained from SEIs shown in Figs. 3 and 4. The relationship between particle size and aging time indicates good linearity between them in logarithmic scale. The volume fraction of precipitates start to increase with aging and saturated at a certain time for each aging temperature reaching an equilibrium composition.

The increase of the precipitate size is driven by two forces. The driving force for the classical nucleation and growth model is a reduction of total chemical free energy by precipitation of nuclei and their subsequent growth. By contrast, the driving force for Ostwald ripening is reduction of the interfacial energy by coarsening. Lifshitz–Slyozov–Wagner (LSW) theory can be used to derive the coarsening kinetics[33]. It describes the particle radius using the following standard equation when we assume Ostwald ripening.

$$\bar{r}^3 - \bar{r}_0^3 = K\,(t - t_0) \tag{9}$$

If we assume initial particle radius r_0 and initial time t_0 are sufficiently small, then

$$\bar{r} \propto t^{1/3} \tag{10}$$

where $\bar{r}$ is the average particle radius at time t and K is a constant, respectively. The saturation of volume fraction indicates depletion of the driving force for precipitation, which is good agreement with conditions to apply LSW theory. Particle radius and aging time obey proportional relationship whose gradient approximately 1/3. It is noted that lower aging temperature achieves a higher volume fraction of γ' precipitates.

Figure 6 shows the TEM bright field images for specimens aged at 1173 K for 10, 24 and 96 h. For the specimen aged for 10 h, black contrast is clearly observed around the γ' parti-

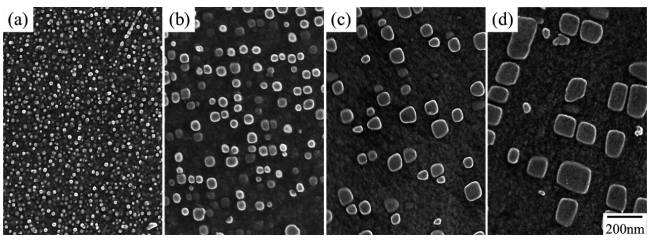

Fig. 4 FE-SEM micrographs of Inconel X-750 aged at 1073 K for 1 h (a), 24 h (b), 96 h (c) and 750 h (d).

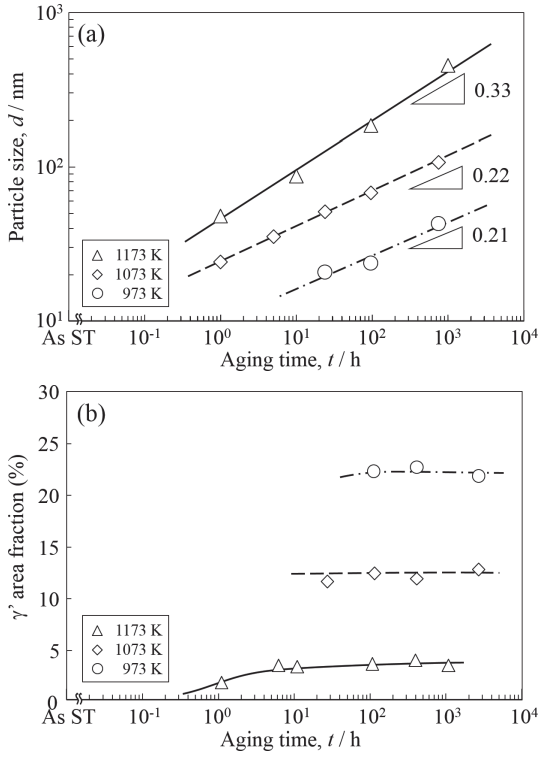

Fig. 5 Plots of particle size (a) and γ' area fraction (b) vs. aging time for Inconel X-750 at temperatures between 973 and 1173 K.

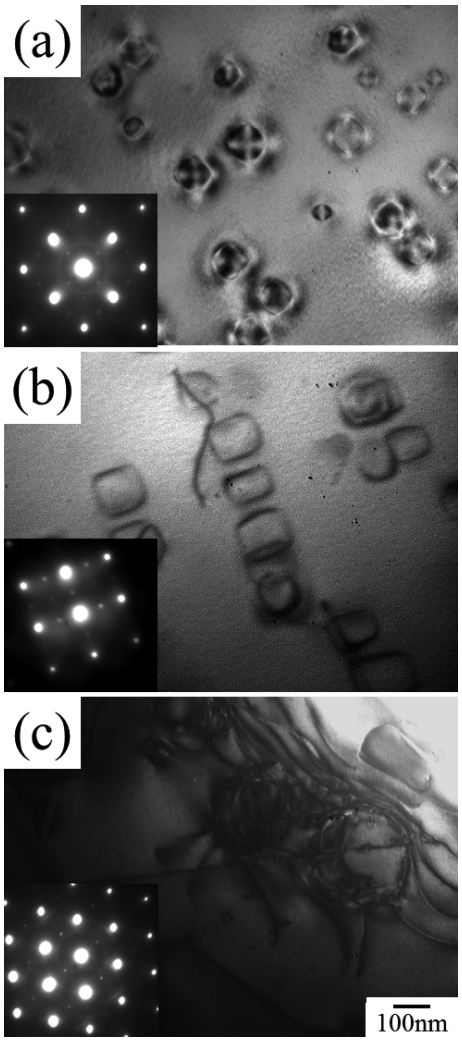

Fig. 6 Bright field images of Inconel X-750 aged at 1173 K for 10 h (a), 24 h (b) and 96 h (c).

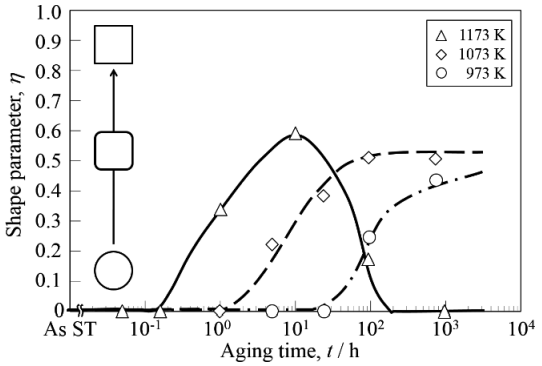

Fig. 7 Plot of the shape parameter vs. aging time for Inconel X-750 at temperatures between 973 and 1173 K.

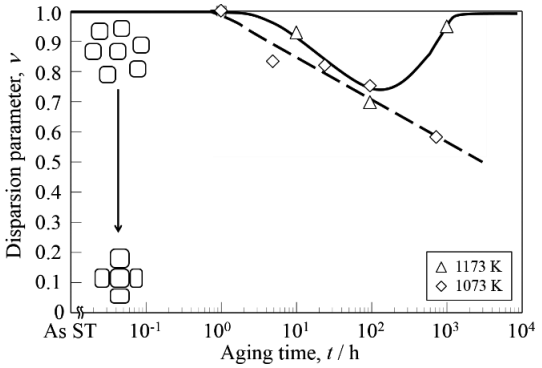

Fig. 8 Plot of dispersion parameter vs. aging time for Inconel X-750 at temperatures between 1073 and 1173 K.

cles, which might be an elastic strain field due to lattice misfit. This result is consistent with the elastic theory based numerical simulation results reported by Shen *et al.*[34] For the 24 h aged specimen γ' particles begin to induce misfit dislocation at the γ/γ' interface and are punched-out, i.e., interfacial dislocation develops into the matrix. For the specimen aged for 96 h, a high density of misfit dislocations surrounds the γ' particle.

The γ/γ' interface clearly becomes incoherent after prolonged high temperature exposure. The morphological changes are also observed in specimens aged at 973 K. Because aging conditions in this alloy are sufficiently long to attain the chemical equilibrium, the occurence of these morphological changes of γ' precipitates is the evidence of the existence of lattice misfit.

3.2 Quantification of γ' morphology

Microstructure observations reveals that the γ' morphology is dramatically changed upon isothermal aging at 1073–1173 K as shown in Figs. 3 and 4. These morphological changes with aging were quantified using three dimensionless parameters.

Figure 7 shows the change in shape parameter η as a function of aging time. Notably again a large η indicate more cuboidal particles. At 1173 K this parameter initially increases at 1 h of aging and reaches a maximum of 0.6 at approximately 10 h. After that it gradually decreases to 100 h then falls into 0 at 300 h. At 1073 K this parameter starts to increase at 10 h and reaches maximum at 100 h. It does not decrease over 1000 h of aging. Starting increase in shape parameter is corresponding to the start to form cuboidal. Starting decrease indicates collapsing cuboidal shape. A decrease to 0 indicates the transformation to irregular shape particles as the result of incoherence of γ/γ' interface.

Figure 8 shows the change in dispersion parameter ν with increasing aging time. At 1173 K, this parameter decreases at 1 h of aging and reaches a minimum of 0.7 at approximately 100 h. It then recovers to almost 1 at 1000 h. At 1073 K, this parameter also decreases at 1 h and continues to decrease beyond 750 h. The specimens aged at 1173 K and 1073 K show a similar decreasing starting point at 1 h despite the 100 K difference in temperature. Moreover, the specimen aged at 1073 K has a smaller minimum value, which indicates stronger interaction among γ' particles, promoting the formation of particle groups. More particles form groups and the dispersion parameter decreases with coarsening until 1173 K/1000 h, at which point the dispersion parameter rapidly increases with coalescence.

Figure 9 shows the change in coalescence parameter σ^* as a functions of aging time. These parameters for specimens aged at both 1173 K and 1073 K gradually increase during

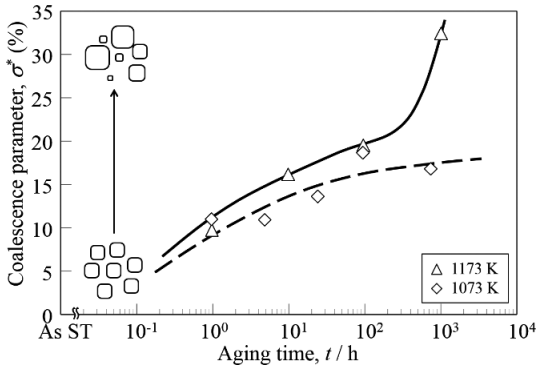

Fig. 9 Plot of coalescence parameter vs. aging time for Inconel X-750 at temperatures between 1073 and 1173 K.

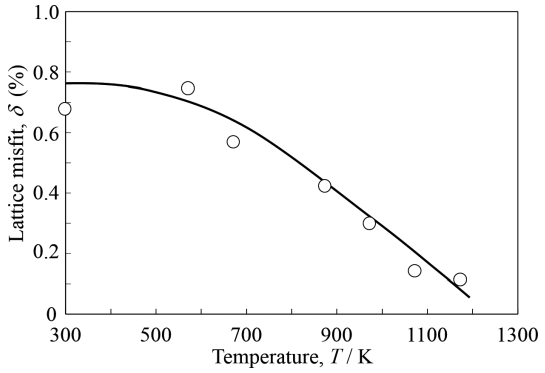

Fig. 11 Relationship between lattice misfit and temperature for Inconel X-750 pre-aged at 1173 K/96 h.

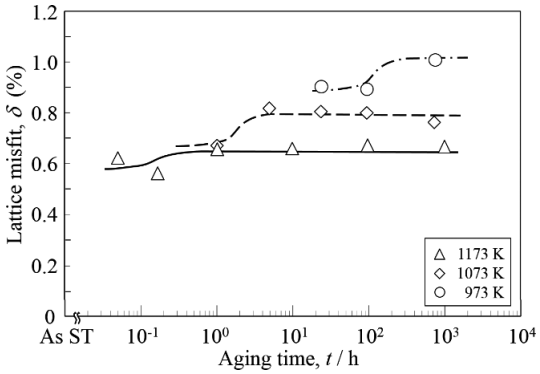

Fig. 10 Plot of lattice misfit measured at RT vs. aging time for Inconel X-750 at temperatures between 973 and 1173 K.

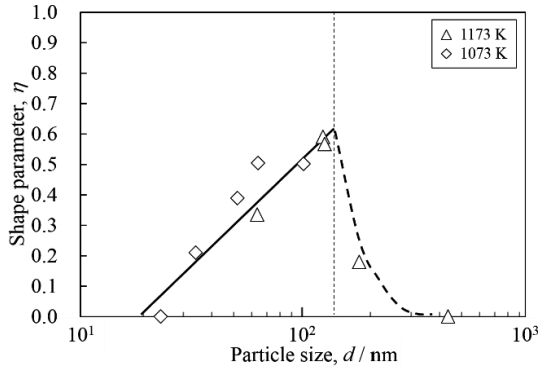

Fig. 12 Plot of shape parameter vs. particle size for Inconel X-750 aged at 1073 and 1173 K.

aging, which might be a result of homogeneous nucleation and reaching pure the point of Ostwald ripening corresponding to $\sigma^* = 0.219$. An anomalous increase point is also observed at 1173 K/300 h. This is the evidence of coarsening mode resulting from macroscopic coalescence. The specimen aged at 1073 K remains in mild coarsening mode for aging times longer than 750 h, which is consistent with the non-irregular shape of the particles shown at Fig. 4(d).

3.3 X-ray diffraction

Figure 10 shows the change in the lattice misfit between the γ and γ' phases with increasing aging time as measured at RT. In this alloy, the lattice parameters of the γ' phase are larger than those of the γ phase under all aging conditions, which result in a positive lattice misfit; by contrast most cast Ni-based superalloys have negative lattice misfit[1]. Because Inconel X-750 alloy does not include elements, associated with solid solution hardening such as Mo or W, the lattice of the matrix phase does not dramatically expand[35]. Specimens aged at higher aging temperature exhibit lower increase in lattice misfit during aging at early stage of precipitation and subsequent saturation. The saturated lattice misfit is approximately 1.0% at 973 K, 0.8% at 1073 K and 0.6% at 1173 K.

Figure 11 shows the change in lattice misfit for the specimen pre-aged at 1173 K/96 h as a function of measurement temperature. The microstructure of these specimen is shown in Fig. 3 (c). The lattice misfit of the sample is approximately 0.6% at RT and decreases to 0.1% at 1173 K. These results clarify that the lattice misfit strongly depends on not only aging temperature but also measurement temperature. The temperature dependence of the lattice misfit is equivalent to the difference in the coefficients of thermal expansion (CTEs) between the γ and γ' phases. The CTE of γ is known to be often higher than that of the γ' phase resulting in negative temperature dependence regardless of the alloy's composition and the sign of lattice misfit. This result suggests that we achieved to attain less than 0.1% lattice misfit.

4. Discussion

4.1 Morphological changes in γ' precipitates

The morphological changes in γ' precipitates were evaluated using three individual parameters that describe the shape, dispersion and coalescence. These approaches have revealed concrete morphological changes as discussed below.

The changes of the γ' particles' shape with coarsening are divided into four steps. First, γ' particles are initially spherical to retain interfacial energy with little misfit strain storage. In this step, interfacial energy is the dominant factor of particle shape. Second, γ' particles become cuboidal with coarsening under constraint by lattice misfit. Figure 12 shows a plot of the shape parameter vs. the average particle size of the specimens aged at 1073 and 1173 K. This figure clearly shows that larger particles have a shape parameter, indicating that they exhibit a more cuboidal shape until reaching a critical particle size regardless of aging temperature. Strain ener-

gy that originates form lattice misfit becomes the dominant factor in this step; strain energy accumulates around the particles during coarsening, resulting in a cuboidal shape. Shape parameter η reaches maximum when the particle size reaches the critical critical value at approximately 120 nm, and then decreases. The particles lose their cuboidal shape as the third step and finally completely collapse into an irregular shape in the fourth step.

A decrease or maximization of the shape parameter is attributed to induced misfit dislocations as shown in Fig. 6. Maximization of the shape parameter and induction of the misfit dislocation occur at the same time at 1173 K/24 h. Interfacial misfit dislocations have been reported to affect the elastic field around a particle[32,36], which might trigger a transformation to spherical shapes. The transformation to irregular shapes is not achieved through loss of cuboidal shape; it is attributed to the beginning of coalescence, indicated as an anomalous increase of the coalescence parameter σ*. The possibility exists that misfit dislocations promote coalescence because coalescence requires a short incubation time to coarsen. The critical condition required or mechanism of misfit dislocation induction at γ/γ' interfaces remains unknown and requires further investigation[36].

A change in γ' dispersion is also divided into three steps. First, γ' precipitates are homogeneously nucleated and dispersed at the early stage of aging. Second, they start to form aligned or arrayed groups and undergo "localized" dispersion corresponding to the decrease of dispersion parameter ν. Finally, they become homogeneous dispersion again through coalescence of particles that form groups, consistent with recovery of the dispersion parameter ν. A decrease of the dispersion parameter begins almost simultaneously with γ' coarsening and/or increasing of the shape parameter η. The formation of groups can also be reasonably considered originate from retention of strain energy[20,21].

4.2 Interaction among morphological features

The γ' morphology is summarized as follows. Initially, γ' particles precipitate with a spherical shape and a homogeneous dispersion; the morphologies are referred to as "spherical". They coarsen, resulting in "cuboidal" shape and "localized" dispersion concurrently, regardless of the depletion of the driving force for γ' precipitation. Reaching the limit size of coherency, the γ' particles become too large to storage elastic strain energy around the particles, and then begin to induce misfit dislocations. This might be the start of incoherence between the γ and γ' phases. Finally, coalescence of γ' particles occurs resulting in a distinctive shape and a homogeneous dispersion.

This morphological changes in γ' precipitates is observed in the temperature range from 973 to 1173 K. The kinetics and temperature dependence of the γ' morphology is summarized in Fig. 13, which also includes the experimentally determined precipitation start line of the alloy. Figure 13 shows that earlier morphological changes occur at higher aging temperatures, which means the morphological changes are a thermally activated process that contributes to coarsening of the particles.

However, only a "localized" start line indicates typical temperature dependence, referred to as the C-curve. "Localized"

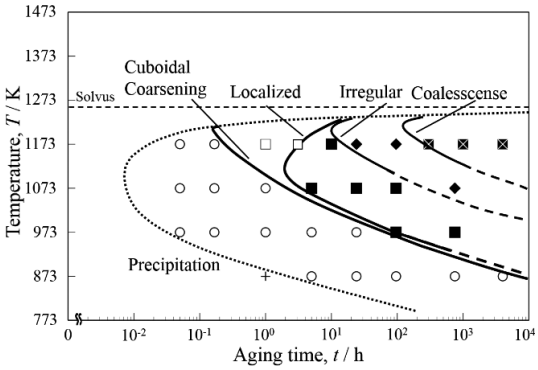

Fig. 13 Morphology map of γ' precipitates during isothermal aging for Inconel X-750 together with the precipitation start line for the alloy. Circles (○), squares (□, ■) and rhombus symbols (◆) indicate spherical, cuboidal and irregular morphology of γ' particles, respectively. Open symbols (○, □) and solid symbols (■, ◆) indicate that the γ' dispersion is heterogeneous and localized.

phenomena depend on not only the aging temperature or particle size but also on the volume fraction, i.e., the incidence of particles facing each other[18]. That is, a large volume fraction of γ' precipitate facilitates the "localized" phenomenon. These are evidence of the existence of elastic field and its interaction around particles. Even in wrought superalloys with a low volume fraction approximately 5%, elastic interaction cannot be ignored in descriptions of the growth and coarsening process.

4.3 γ' morphology and lattice misfit

Although the γ' morphology changes dramatically, the extent of lattice misfit between the γ and γ' phases slightly increases at the early stage of aging, and then retain almost constant with isothermal aging. The lattice misfit depends on the chemical composition of the γ and γ' phases. The slight increase in misfit should correspond to changes in composition of the γ and γ' phases with growth, and the increase should stop due to depletion of driving force to growth. The processes of composition changes of the matrix and precipitate phases were not determined, however, all of the morphological changes occurred after the composition change is completed. Lahrman *et al.*[32] showed that the magnitude of lattice misfit decreased by approximately 30% when the interface between the γ and γ' phases became incoherent because of the release of misfit stress. However, this phenomenon was not detected in this study even though a high density of misfit dislocations was induced and misfit strain was released. At lower aging temperatures, where larger lattice misfit is achieved, the morphological change from spherical to cuboidal is not accelerated or enhanced as shown in Fig. 12. This result indicates that the morphological change might strongly depend on the particle size and is less related to the magnitude or sign of lattice misfit. Moreover, the absolute value of lattice misfit is small (~0.1%) at high temperature in the alloy. This result might support another dominant factor such as local segregation[37], elastic constant inhomogeneity[38–40], volume fraction of precipitates, or interfacial energy.

The other feature of this study is the great requirement to measure the lattice misfit at aging temperature compared to cast superalloys with a large volume fraction of γ' phase. The lattice misfit of both wrought and cast alloys exhibit a nega-

tive temperature dependence; however, the degree of temperature dependence in wrought alloys is much higher than that in cast alloys. The difference in lattice misfit between 300 K and 1173 K is approximately 0.8% in Inconel X-750, whereas it is 0.2% in several cast superalloys[6,8,41,42]. The difference in the degree of temperature dependence might be due to alloys design for forgeability at high temperatures (e.g. wrought alloys contain less refractory metals such as Ru, Re, W and Mo) enabling both a low volume fraction of γ' phase at high temperature and an intermediate volume fraction at low temperatures. The γ' phase is destabilized at high temperatures corresponding to the strong temperature dependence of chemical composition of the matrix and the precipitates. By contrast, cast alloys contain much higher fractions of γ' forming elements and refractory metals imparting the alloys with high strength and good stability even at high temperatures. This possibility suggests that we should consider the strength of temperature dependence of the lattice misfit when investigating lattice misfit of wrought Ni-based superalloys.

5. Conclusions

The lattice misfit between the γ/γ' phases and the morphology of γ' phase in a wrought Ni-based superalloy, Inconel X-750 with a γ' volume fraction less than 20% were examined.

(1) γ' morphology was quantitatively evaluated successfully using individual shape, dispersion and coalescence parameters.
(2) The shape of the γ' particles becomes cuboidal and subsequently changes to irregular during aging. This change correspond to the retention of strain energy and to its subsequent relief inducing misfit dislocation.
(3) The dispersion of the γ' phase becomes localized and then recovers. Localization occurs simultaneously with the formation of cuboidal shapes. The kinetics and magnitude of this "localization" phenomenon may depend on the volume fraction of precipitates.
(4) Coalescence appears to occur when the precipitate size reaches a critical size, irregular shapes and a homogeneous dispersion are thereafter formed again.
(5) The change in γ' morphology occurs at all of the studied temperatures, although the lattice misfit retains during isothermal aging.
(6) The magnitude of lattice misfit in this alloys is very low at aging temperature, which suggests that another factor affects the γ' morphology.

Acknowledgements

The authors wish to thank Professor S. Onaka, Dr. N. Takata and Mr. K. Izumi for inspiring discussion. Dr. Y. Miyajima is thanked for the help on the microstructure observation with FE-SEM. This work was supported by a Grant-in-Aid for JSPS Research Fellow Number JP2611840, Japan.

REFERENCES

1) T.M. Pollock and S. Tin: J. Prop. Pow. **22** (2006) 361–374.
2) F. Sun, Y.F. Gu, J.B. Yan, Y.X. Xu, Z.H. Zhong and M. Yuyama: J. Alloy. Compd. **687** (2016) 389–401.
3) R. Viswanathan, J. Shingledecher and J. Hawk: ECCC (2009) 31–42.
4) X.Z. Qin, J.T. Guo, C. Yuan, J.S. Hou, L.Z. Zhou and H.Q. Ye: Mater. Sci. Eng. A **543** (2012) 121–128.
5) J. Zrnik, P. Strunz, V. Vrchovinsky, O. Muransky, Z. Novy and A. Wiedenmann: Mater. Sci. Eng. A **387–389** (2004) 728–733.
6) D.A. Grose and G.S. Ansell: Metall. Trans. A **12** (1981) 1631–1645.
7) R.A. MacKay and M.V. Nathal: Acta Metall. Mater. **38** (1990) 993–1005.
8) T. Sugui, W. Minggang, Y. Huichen, Y. Xingfu, L. Tang and Q. Benjiang: Mater. Sci. Eng. A **527** (2010) 4458–4465.
9) M. Fährmann, P. Fratzl, O. Paris, E. Fährmann and W.C. Johnson: Acta Metall. Mater. **43** (1995) 1007–1022.
10) R.A. Ricks, A.J. Porter and R.C. Ecob: Acta Metall. **31** (1983) 43–53.
11) S. Onaka, N. Kobayashi, T. Fujii and M. Kato: Mater. Sci. Eng. A **347** (2003) 42–49.
12) M.E. Thompson, C.S. Su and P.W. Voorhees: Acta Metall. Mater. **42** (1994) 2107–2122.
13) X. Zhao, S.P.A. Bordas and J. Qu: J. Mech. Phys. Solids **81** (2015) 1–21.
14) P.W. Voorhees, G.B. Mcfadden and W.C. Johnson: Acta Metall. Mater. **40** (1992) 2979–2992.
15) A.G. Khachaturyan, S.V. Semenovskaya and J.W. Morris, Jr.: Acta Mater. **36** (1988) 1563–1572.
16) S.V. Prikhodko and A.J. Ardell: Acta Mater. **51** (2003) 5021–5036.
17) A. Maheshwari and A. Ardell: Scr. Mater. **26** (1992) 347–352.
18) A.C. Lund and P.W. Voorhees: Acta Mater. **50** (2002) 2585–2598.
19) X. Zhao, R. Duddu, S.P.A. Bordas and J. Qu: J. Mech. Phys. Solids **61** (2013) 1433–1445.
20) C.H. Su and P.W. Voorhees: Acta Mater. **44** (1996) 1987–1999.
21) C.L. Qiu and P. Andrews: Mater. Charact. **76** (2013) 28–34.
22) A.K. Sinha and J.J. Moore: Metallography **19** (1986) 75–86.
23) P.K. Venkiteswaran, M.W.A. Bright and D.M.R. Taplin: Mater. Sci. Eng. **11** (1973) 255–268.
24) G.R.X. de Souza, S.B. Gabriel, J. Dille, D.S. dos Santos and L.H. de Almeida: Mater. Sci. Eng. A **564** (2013) 102–106.
25) J.A. del Valle, A.C. Picasso, I. Alvarez and R. Romero: Scr. Mater. **41** (1999) 237–243.
26) T. Kekkonen and H. Hänninen: Corros. Sci. **25** (1985) 789–803.
27) A.K. Sinha and J.J. Moore: Metallography **19** (1986) 87–98.
28) J.P. MacSleyne, J.P. Simmons and M. De Graef: Acta Mater. **56** (2008) 427–437.
29) J.S. Van Sluytman and T.M. Pollock: Acta Mater. **60** (2012) 1771–1783.
30) L. Nguyen, R. Shi, Y. Wang and M. De Graef: Acta Mater. **103** (2016) 322–333.
31) X.P. Tan, J.L. Liu, X.P. Song, T. Jin, X.F. Sun and Z.Q. Hu: J. Mater. Sci. Technol. **27** (2011) 899–905.
32) D.F. Lahrman, R.D. Field, R. Darolia and H.L. Fraser: Acta Metall. **36** (1988) 1309–1320.
33) R.S. Moshtaghin and S. Asgari: Mater. Des. **24** (2003) 325–330.
34) C. Shen, J.P. Simmons and Y. Wang: Acta Mater. **54** (2006) 5617–5630.
35) R.A. MacKay, T.P. Gabb, A. Garg, R.B. Rogers and M.V. Nathal: Mater. Charact. **70** (2012) 83–100.
36) H. Long, H. Wei, Y. Liu, S. Mao, J. Zhang, S. Xiang, Y. Chen, W. Gui, Q. Li, Z. Zhang and X. Han: Acta Mater. **120** (2016) 95–107.
37) Y. Chen, R. Prasath babu, T.J.A. Slater, M. Bai, R. Mitchell, O. Ciuca, M. Preuss and S.J. Haigh: Acta Mater. **110** (2016) 295–305.
38) M. Cottura, Y.L. Bouar, B. Appolaire and A. Finel: Acta Mater. **94** (2015) 15–25.
39) M. Kato, T. Fujii and S. Onaka: Mater. Trans., JIM **37** (1996) 314–318.
40) A.J. Ardell: Philos. Mag. **94** (2014) 2101–2130.
41) M.V. Nathal, R.A. Mackey and R.G. Garlick: Mater. Sci. Eng. **75** (1985) 195–205.
42) M. Fährmann, J.G. Wolf and T.M. Pollock: Mater. Sci. Eng. A **210** (1996) 8–15.